



**Budapest University of Technology and Economics**  
Doctoral School of Informatics  
Department of Telecommunications and Artificial Intelligence

# Time synchronization in packet switching networks

THESIS BOOKLET

*Ph.D. candidate*  
Gergely Hollósi

*Supervisor*  
Pál Varga, Ph.D.

February 24, 2025

# Introduction

The need for synchronizing clocks within computer networks has a lengthy history, but contemporary time synchronous networks present novel challenges to synchronization accuracy. Accurate synchronization is gaining increased attention in practical industrial internet-of-things (IIoT) applications and various use-cases, such as real-time scenarios like nuclear fusion control, mobile communication (5G/6G), substation automation, and modern manufacturing plants [1, 2]. The recent IEEE 1588-2019 standard [3], commonly known as the Precision Time Protocol (PTP), addresses the challenge of sub-microsecond accurate clock synchronization over communication networks. Precise time synchronization is essential also in indoor and outdoor localization systems, where clocks in base stations (referred to as anchors) need synchronization with each other or a global logical clock. Techniques like time difference of arrival in 5G networks [4, 5] or ultra-wideband (UWB) systems [6, 7, 8] require synchronization of frequency drifts at the nanosecond level. Localization is a critical mechanism for determining the locations of data sources in wireless sensor networks (WSN), autonomous robots, or the Internet of Things (IoT) [9].

In the realm of accurate and precise time synchronization, three prominent technologies come to mind: the Global Navigation Satellite System (GNSS), Precision Time Protocol (PTP), and Ultra-Wideband technology (UWB). The interconnection of time synchronization and localization is undeniable, as most positioning methods favor time-of-flight or time-difference-of-arrival techniques, requiring accurate time measurements in transceivers. This dissertation focuses on the precise time synchronization in packet-switched networks – precise in aiming for high precision (low variance) beyond accuracy, and packet-switched because the findings can generally be applied to time synchronization of digital clocks through any packet-switched communication systems.

The dissertation discusses three different topics separated in four thesis groups, all topics concentrating on clock synchronization issues. **Thesis group 1** presents a state-of-the-art time division method for increasing the number of time measurements in ultra wide band networks resulting in more information about the clock state of the nodes in the UWB network, facilitating more accurate ranging and time synchronization. The chapter also presents, that the framing structure perform similar ranging metrics as the method of the IEEE 802.15.4 standard.

The connection between the high accuracy requirements of the time measurement in wireless localization (e.g. ranging) and the time synchronization solutions raises the question: is UWB applicable to synchronize controllable PTP clocks? **Thesis group 2** proposes a specific implementation based on the well-known DW1000

chipset pointing out the problem of chip level clock domain change.

**Thesis group 3** handles the topical problem of unknown propagation delay variations over wireless channels, which deviates the performance of clock synthonization (frequency synchronization) algorithms. While a couple of methods are proposed for the problem, the linearity of the dynamic and measurement models makes it possible to apply Kalman-filtering, resulting is superior performance – however, Kalman-filtering requires the estimate of the propagation delay variance to be the optimal estimator. The chapter lend a method from machine learning to estimate parameters in latent space problems, which results in the optimal estimate of both the states and the measurement variance.

Measurement noise variance, which is mostly covered by the name packet delay variation (PDV) in wired networks, is also a problem in the Precision Time Protocol. While numerous technical solution has been proposed and implemented – like transparent clocks, or the White Rabbit Project – to overcome the unknown delays of the synchronizing packets over the network, statistical methods always can help to make optimal estimation of the clock state by inferring the measurement noise on-the-fly. **Thesis group 4** proposes the Adaptive Kalman Filter to adaptively estimate the measurement noise, by applying a measurement model with time-invariant measurement noise covariance matrix. It is shown, that the method supersedes existing state-of-the-art solutions for estimating the clock state.

# Research objectives

My research was driven by previous investigations in real-time indoor localization. However, it has become apparent that the findings are not only relevant to this specific field but also extend to the broader domain of time synchronization. Identifying a lack of studies in adaptive filtering-based clock synchronization has highlighted a gap in estimation theory relating to clock synchronization. Furthermore, to highlight the synergies of ultra wide band systems and Precision Time Protocol, an experiment was conducted to validate the effectiveness of ultra-wideband communication in synchronizing remote PTP clocks wirelessly with remarkable accuracy and precision. More specifically, the primary research objectives include:

- Exploring potential methods for augmenting the ranging and synchronization capabilities of ultra-wideband devices to improve the temporal resolution and accuracy of both indoor and outdoor localization systems.
- Analyzing the distribution of receive timestamps in both wired and wireless systems utilizing standard propagation models and simulations.
- Proposing techniques for real-world measurement of receive timestamp distributions in ultra-wideband and Precision Time Protocol-based systems.
- Developing algorithms to adaptively estimate the variance of measurement noise to optimize the filtering process for clock state and frequency synchronization.
- Investigating the integration of Precision Time Protocol and ultra-wideband communication to furnish a precise wireless medium for synchronizing PTP clocks.

# Methodology

As the thesis covers different areas of research gaps that needs different approaches, I carefully chose the approach fitting to the given problem set. Throughout the research, I collectively applied the DSR (Design Science Research) [10] methodology. A variety of formal and practical methodologies are employed. Bayesian estimation serves as the foundation for all thesis groups; however, Thesis groups 3 and 4 extensively utilize Kalman filtering to address Bayesian estimation for Gaussian random variables in linear models. Additionally, Thesis group 3 employs Expectation-Maximization to estimate parameters in latent space problems represented as Markov chains, resolving the joint estimation problem by decoupling state estimation from parameter estimation. Moreover, Thesis group 4 utilizes innovation-based covariance matching to estimate measurement noise, while Thesis group 1 employs error propagation analysis using predefined error models. Clock modelling is based on well-established Simple Skew Models and probabilistic state space models. Thesis group 2 uses analytical derivation of clock state after clock domain change.

In Thesis group 3, simulation employs the Saleh-Valenzuela wideband propagation model to generate baseband signals, exploring the distribution of received timestamps through threshold crossing. Meanwhile, Thesis group 4 conducts simulations assuming various noise profiles for receive timestamps, evaluating the proposed solution through estimation variance and Allan variance. Real-world data are also collected to assess the proposed solutions in all Thesis groups, with the data gathering methods detailed within each Thesis.

For evaluation, a number of metrics are employed. In Thesis group 1, ranging error is measured by absolute error. In Thesis group 2, synchronization error is also measured by absolute error. In Thesis groups 3 and 4, clock state estimation is assessed based on state estimation bias and variance, and the Allan variance of the controlled clock is also evaluated.

# Results

## 4.1 Efficient ultra wide band measurement system design

---

**Thesis Group 1** – I have shown that increasing the effective data rate in Ultra Wide Band systems by using a special messaging scheme with larger messages results in a higher ranging rate and more frequently received RX timestamps. I have designed a novel, scalable time-division messaging scheme that provides higher synchronization, ranging and localization rate in ultra wide band systems. I have shown, that the increment in the ranging rate is accompanied by a tiny increment in the ranging error. [C1]

---

The thesis group introduces a messaging framework that optimizes the usage of resources. The advantage is outstanding when it is compared to a classical TWR ranging protocol efficiency. However, this messaging design introduces additional ranging delay while increases the scalability of ToA systems. To justify the virtue of the proposed framework, ranging results are compared with classical distance measurements. The related experimental performance evaluation proves that the introduction of higher ranging time does not affect the ranging accuracy, however drastically increases scalability.

### 4.1.1 Increasing the effective data-rate for enhancing measurement frequency

---

**Thesis 1.1** – I have shown that the increment in effective data rate can be exploited to raise the localization rate (i.e. computed locations per second) using a specific framing structure. The localization rate can increase up to 3 times compared to the classical ranging methods.[C1]

---

Typical UWB packet consists of a synchronization header (SHR), a PHY header (PHR) and the remaining user data (PSDU – PHY Service Data Unit). The SHR part is always transmitted with base rate independent of the data rate, putting

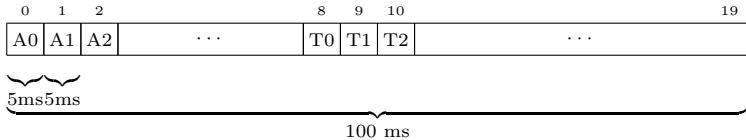


Figure 4.1: The proposed superframe structure. The superframe can be partitioned for an anchor part and a tag part. In the superframe, anchors send their messages in sequential order then the tags send their messages also in sequential order. In the figure, 'A' stands for anchor and 'T' stands for tag. The example shows 8 anchors and 12 tags resulting in a 100 ms long superframe with 5 ms timeslots.

a constant, and rather big overhead to communication. Utilizing longer messages results in increased effective data rate in UWB systems.

The proposed superframe structure can be seen in Fig. 4.1. The structure of the superframe consists of an anchor part and a tag part. During the anchor part, the anchors send their messages, while in the tag phase, tags send their messages. The transmissions happen in sequential order which of course assumes that the devices own some preconfigured identifiers.

The slots in the superframe are 5 ms wide which provides a decent guard time between slots. Since the example uses 8 anchors and 12 tags, the whole superframe is 100 ms long, so in one second 10 of this superframe can be transmitted. The format of the anchor and tag packets can be found in Fig. 4.3.

The main advantage of the proposed solution is that the proposed system provides increased capacity of ranging and localization over the same radio resources. Two measures are computed for both the classical and the novel methods: the *ranging rate* shows the maximum number of ranges (i.e. distance between two devices) that can be measured by the system in a time unit (typically one second), while *localization rate* stands for the same in terms of the maximum number of locations.

To present the results, the calculations were done for 850 kbps data rate, 1024 symbols long preamble, 64 MHz PRF frequency and – in the novel method – for eight anchors. Also, no guard times and no auxiliary frames are involved. Fig. 4.2 shows the cases for all the ranging and only the tag ranges. It is important to emphasize that, in case of localization rate, all the ranges between the anchors and the tags were accounted, providing more robust localization.

With the same assumption, the – theoretic – limit was calculated as

$$\lim_{c_t \rightarrow \infty} \frac{\beta_{\text{novel}}^{\text{loc}}}{\beta_{\text{classic}}^{\text{loc}}} = \frac{5961.54n_{\text{pr}} + 1768405.272}{993.59n_{\text{pr}} + 924439.876} \Big|_{n_{\text{pr}}=1024} = 4.054 \quad (4.1)$$

At limit, using 1024 long preamble, more than 400% increment can be reached in localization rate using the novel method. However, using  $c_t = 20$  tags, the increment is reduced to 306%, which is also an impressive result.

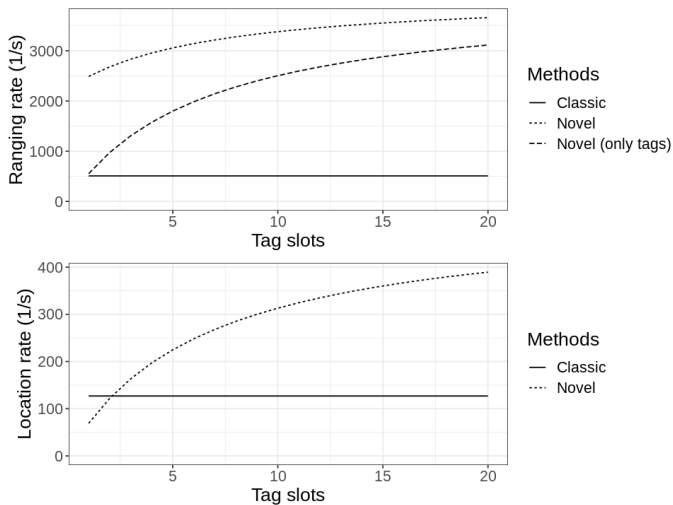


Figure 4.2: Theoretical ranging and localization system capacity against the count of tag slots using 8 installed anchors (higher is better). For details, see text.

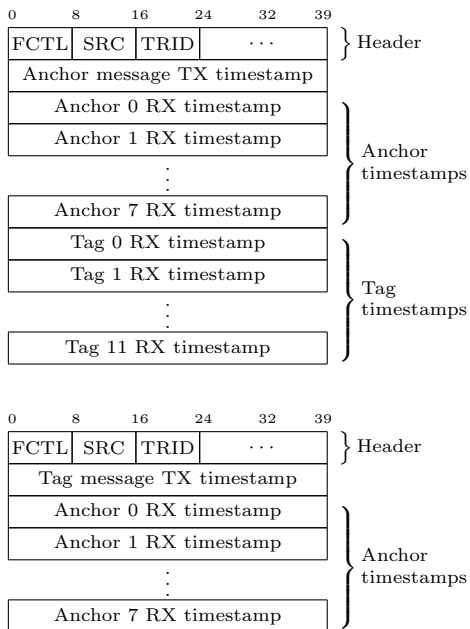


Figure 4.3: The message format of the anchor and tag messages. (top: anchor message, bottom: tag message)

## 4.1.2 Analysis of ranging error

---

**Thesis 1.2** – I have shown that the ranging error in a system presented above slightly increases the ranging error through the frequency drift between the transceivers and the movement of the transceivers. I have derived analytical approximations for the ranging error given a simple skew clock model and linear movements. I have shown that the ranging error can be neglected in typical applications. [C1]

---

The proposed method shows big improvement in the speed of localization, however, the method introduces new kind of errors. Along with the well known errors presented in TWR (timestamping error, nominal frequency error) there arise two other sources of error which require some analysis. One reasoning behind the classical quick ranging message exchange is that this way a roughly static state of the world can be captured, i.e. there is little movement between epochs of message transmissions, and the observed frequency change is negligible. However, in the proposed solution there can be tens of milliseconds between transmissions. The two most important sources of errors are analyzed in this section: the error resulting from the frequency drift of the oscillators and the result of movement between transmissions.

First, we consider the error caused by the frequency drift between the oscillators of the anchor and the tag. Suppose an  $f(t) = f_1 + \Delta \cdot f_1 \cdot t$  linear frequency change (i.e. an SKM model), where  $f_1$  is the nominal frequency of the first device and  $\Delta$  is the relative frequency drift to the nominal frequency. The drift error in the time-of-flight calculation is

$$\epsilon_{TOF}^{\text{drift}} = \Delta \frac{2T(T_D^{(2)})^2 + 4TT_D^{(1)}T_D^{(2)} + T_D^{(1)}(T_D^{(2)})^2 + T_D^{(2)}(T_D^{(1)})^2}{4(2T + T_D^{(1)} + T_D^{(2)})} \quad (4.2)$$

where  $T_d^{(1)}$  and  $T_d^{(2)}$  are the delay durations at the anchor and the tag,  $T$  is the nominal time-of-flight duration and  $\Delta$  is the frequency drift. Fig. 4.4. shows the error in ranging at different drift values in function of a common delay duration (i.e.  $T_d^{(1)} = T_d^{(2)} = T_d$ ).

Suppose some linear movement  $d(t) = d_0 + v \cdot t$ , where  $d_0$  is the distance at the response message (and also the moment of  $t = 0$ ) and  $v$  is the speed of the movement. The time-of-flight error resulting from linear motion is

$$\epsilon_{TOF}^{\text{move}} = \frac{2T(\frac{v}{c})T_D^{(1)} - \frac{v^2}{c^2}T_D^{(1)}T_D^{(2)}}{2(2T + (1 - \frac{v}{c})T_D^{(2)} + T_D^{(1)})} \quad (4.3)$$

where  $T_d^{(1)}$  and  $T_d^{(2)}$  are the delay durations at the anchor and the tag,  $T$  is the nominal time-of-flight duration and  $c$  is the speed of the electromagnetic wave. Fig. 4.5. shows the error at different delay durations in function of the speed of the movement.

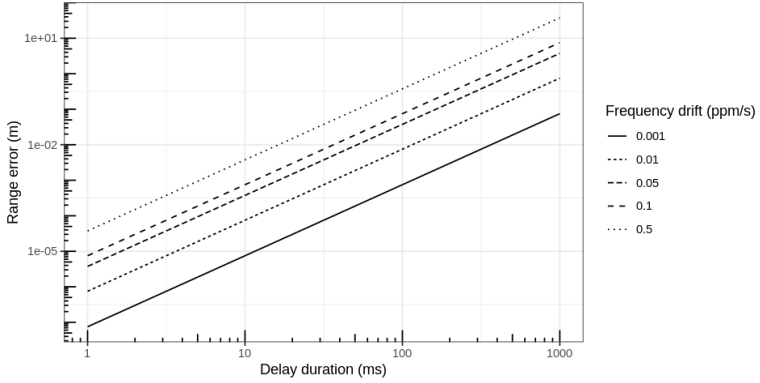


Figure 4.4: The ranging error versus the delay duration at different frequency drift values as a log-log plot. The error is quadratic in the time delay, however, it is in the order of couples of millimeters if the delay is smaller than 100 ms.

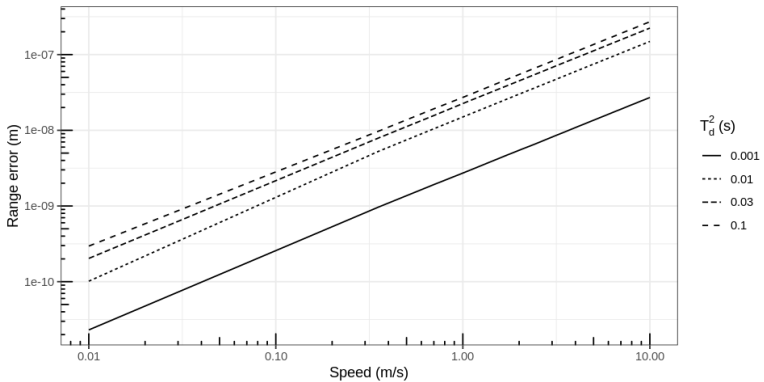


Figure 4.5: The ranging error versus the movement speed at different  $T_d^2$  delay duration as a log-log plot. The delay of  $T_d^1$  is fixed at 10 ms. The error is close to linear in terms of the speed, and is negligible.

## 4.2 Synchronizing PTP clocks using ultra wide band radio

---

**Thesis Group 2** – I proposed, designed, and implemented an ultra wide band-based method to synchronize hardware PTP clocks with high precision. I have shown that the main challenge is the chip-level clock domain change between the PTP clock and the UWB transmitter. To verify the proposed solution for the clock domain change, I designed and implemented a DW1000 chip-based hardware with a PI controller to follow the remote clock. An experiment in an indoor environment shows that the accuracy of the synchronization is in the order of 10 nanoseconds, which is well below the requirements of the strictest synchronicity budget of the 5G system. [J1]

---

The thesis group proposes a method to synchronize local PTP clocks by means of wireless UWB communication. While synchronizing UWB clocks is a widely studied topic, using UWB communication for synchronization of PTP enabled clocks of Ethernet devices is a rarely researched area. The main advantage of the presented method is that the PTP clocks then readily can be used as master clocks in a PTP network.

### 4.2.1 Synchronizing local clock domains

---

**Thesis 2.1** – I have shown that the synchronization of an Ethernet PTP clock to a UWB timestamping clock requires local clock offset synchronization in order to end-to-end synchronize PTP master and slave clocks. I proposed a method to implement clock domain change between a DW1000 chip and an STM PTP configurable clock. [J1]

---

Having two ideal clocks in different clock domains, the general clock model can be written for both clocks:

$$C^{\text{SoC}} = \int_0^t f^{\text{SoC}}(t) dt + o^{\text{SoC}} \quad (4.4a)$$

$$C^{\text{UWB}} = \int_0^t f^{\text{UWB}}(t) dt + o^{\text{UWB}} \quad (4.4b)$$

Here  $C$  is the actual clock counter value,  $f(t)$  is the actual frequency,  $o$  is the offset of the clock and  $t$  is the time. Using  $f^{\text{SoC}}(t) = f^{\text{UWB}}(t)$  and subtracting (4.4b) from (4.4a):

$$C^{\text{SoC}} = C^{\text{UWB}} + (o^{\text{SoC}} - o^{\text{UWB}}) = C^{\text{UWB}} + \Delta o \quad (4.5)$$

where  $\Delta o$  is the offset between the SoC and the UWB chip clocks. However, even with common clock source the offsets in each clock domain cannot be controlled, since the PLLs (Phased Locked Loop) and other circuits make the clock initialization somewhat stochastic, so  $\Delta o$  can change at each reset. Denote  $\Delta o_m$  the offset at the master and  $\Delta o_s$  the offset at the slave. Define

$$\begin{aligned} t_1 &= C_1^{\text{UWB}} + \Delta o_m \\ t_2 &= C_2^{\text{UWB}} + \Delta o_s \\ t_3 &= C_3^{\text{UWB}} + \Delta o_s \\ t_4 &= C_4^{\text{UWB}} + \Delta o_m \end{aligned} \tag{4.6}$$

Combine (4.6) with the PTP offset equation, which yields

$$\Delta t = C_2^{\text{UWB}}(t) - C_1^{\text{UWB}}(t) + \Delta o_s - \Delta o_m - \frac{C_2^{\text{UWB}}(t) - C_1^{\text{UWB}}(t) + C_4^{\text{UWB}}(t) - C_3^{\text{UWB}}(t)}{2}$$

Unfortunately, the difference  $\Delta o_m - \Delta o_s$  is unknown and dependent on the initial offset of the clock, which is mainly random. Ideally,  $\Delta o_m$  should equal  $\Delta o_s$ , and there shall be some process providing constant  $\Delta o$  offsets. To achieve this, some kind of synchronization facility needs to be provided by the UWB transmitter (e.g. DW1000 chip is able to reset the internal timebase triggered by an external pulse).

## 4.2.2 Synchronizing local PTP clock using ultra wide band radio

---

**Thesis 2.2** – I evaluated the proposed method of clock domain change between an STM PTP clock and a DW1000 chip using end-to-end PPS clock offset measurement with a PI controller-based clock servo in an indoor environment. I presented that the synchronization accuracy is in the order of 10 nanoseconds. [J1]

---

The implementation is based on a STM32F407 SoC, which is a powerful, widely used ARM Cortex M4-based device used in embedded systems. The chip has an Ethernet MAC with a built-in frequency tunable PTP clock, which is able to timestamp RX and TX events on the MAC layer. The UWB communication is provided by the well-known Qorvo DW1000 chip, which has excellent timestamping and external synchronization capabilities. Fig. 4.6 shows the connections between the components. External synchronization is implemented by a special SYNC signal in the DW1000 chip. There are two modes used: one-shot transmit synchronization mode (OSTS) and the one-shot timebase reset (OSTR).

After reaching the steady state, 1000 measurements were made by a DSO-X 3054A oscilloscope, using the Pulse Delay Measurement function to analyze and

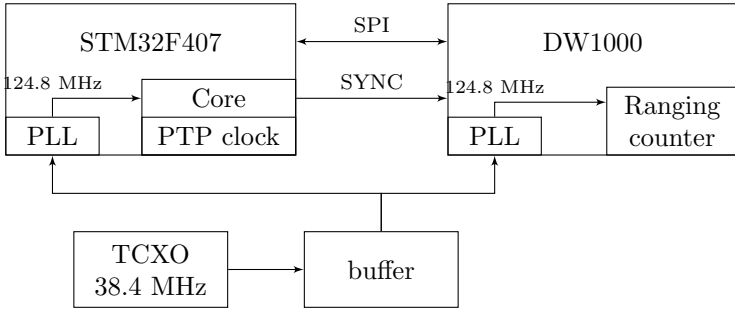
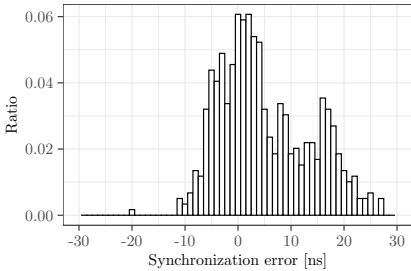
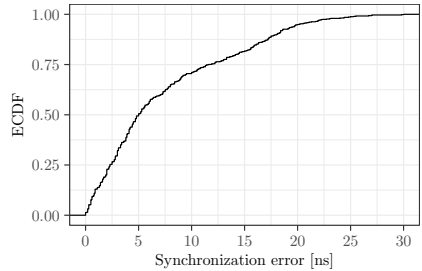


Figure 4.6: The synchronization circuit for evaluating the clock synchronization algorithm. The SoC (STM32F407) and DW1000 UWB transmitter are communication through an SPI interface, and the clock synchronization is performed by the Sync signal. The ranging counter and the SoC system clock (and also the PTP clock) are running on 124.8 MHz.



(a) Histogram of the measured errors



(b) The empirical cumulative distribution plot of the absolute error

Figure 4.7: Distribution of the error measured between the two PPS signals. The histogram is based on 1000 sync cycle after the controller has locked.

record the delay between the PPS signals of the master and slave PTP clock. The result can be seen in Fig. 4.7 as a histogram.

## 4.3 Measurement distribution adaptive synchronization in Ultra Wide Band systems

---

**Thesis Group 3** – By modeling, simulating, and analyzing real measurements of the distribution of receive timestamps in Ultra Wide Band systems, I have shown, that the distributions are diverse and potentially multimodal. I have proposed an adaptive filter to establish the frequency synchronization between the communicating parties by simultaneously estimating the frequency drift and the measurement noise. [C2][C3]

---

The ultra wideband (UWB) technology made it possible to achieve precise, centimeter based asset localization by measuring the exact receive timestamp of incoming messages. The acquired receive timestamp in ultra wide band systems itself is insufficient for localization, e.g. two-way ranging make use of a couple of transmit and receive timestamps. While statistical inference is always carried out assuming Gaussian distribution on the receive timestamps, e.g. using Kalman filters or extended Kalman filters to estimate range or clock drift implicitly presume Gaussian distribution on the measured values, no trace of other claims on the distribution can be found in the literature.

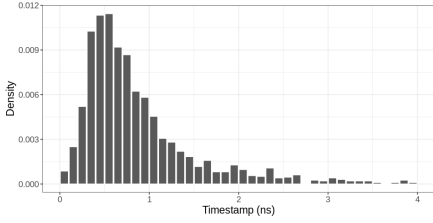
### 4.3.1 Modeling the distribution of received timestamps in ultra wide band systems

---

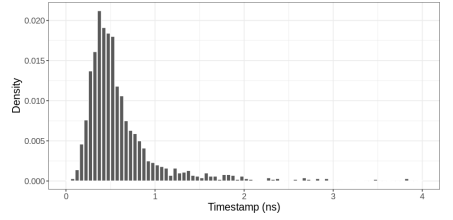
**Thesis 3.1** – Using the recommended wide-band channel model of IEEE 802.15.4a standard based on the wide-band Saleh-Valenzuela model, I have shown that the distribution of the error of receive timestamps does not follow a normal distribution by presenting asymmetric parametric distributions with higher likelihood values. [C2]

---

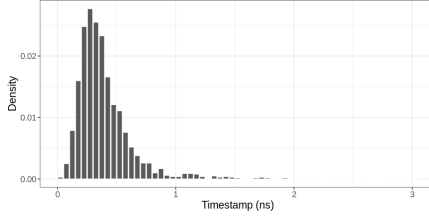
The standard propagation model used in UWB systems is the model proposed in the final report of the IEEE 802.15.4a channel model [11]. Theoretically, to model the distribution of the receive timestamps in UWB systems, the channel model of the ultra wide band propagation and the timestamping process shall be combined to derive the exact distribution of the receive timestamps. The channel model uses a classic ray-tracing model, however, it assumes that the rays arrive in clusters, so



(a) Root raised cosine filter, alternative PDP



(b) Butterworth filter, alternative PDP



(c) Butterworth filter, original PDP

Figure 4.8: Distribution of the receive timestamps based on the simulation of 2000 samples in each scenario.

the impulse response is a double sum, i.e.

$$h(t) = \sum_{l=0}^L \sum_{k=0}^{K_l} a_{k,l} e^{j\phi_{k,l}} \delta(t - T_l - \tau_{k,l}) \quad (4.7)$$

where  $L$  is the number of clusters,  $K_l$  is the number of components in the cluster, which is dependent on the actual cluster. The  $a_{k,l}$  and  $\phi_{k,l}$  are the attenuation and the phase of a component. The  $T_l$  is the delay of the  $l$ -th cluster and  $\tau_{k,l}$  is the delay of a component.

The cluster arrival times make up a Poisson-process with mixture, and the report presents different the power delay profiles for different environments. Finally, small-scale fading is controlled by a Nakagami distribution. Based on the channel impulse response, the received signal can be simulated by convolving the channel impulse response with the impulse response of the pulse shaping filter (e.g. a raised cosine filter or Butterworth filter). The timestamping is done by defining a threshold, and the method searches for the first pulse in the received signal crossing this threshold.

Figure 4.8 shows the result of the simulations. Three scenarios were investigated, the alternative PDP with root raised cosine (RRC) pulse and with Butterworth pulse, and the original PDP with Butterworth pulse. For the RRC pulse, some delay compensation was required because of the non causality of the filter. As it can be seen, the distributions are asymmetric and skewed not like the Gaussian

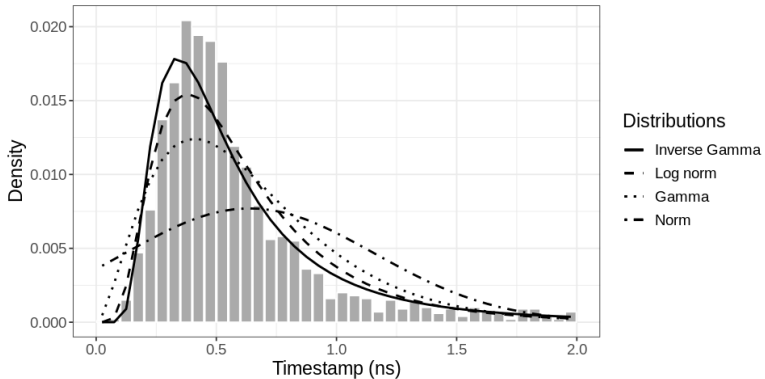


Figure 4.9: Maximum likelihood estimates of different asymmetric probability distributions versus the empirical probability density in case of the Butterworth pulse for the alternative PDP. It is readily visible, that the distribution is far away from a Gaussian distribution.

distribution. For each scenario, the distributions seems similar, but the parameters are somewhat different.

For the skewed distribution, three well-known candidate distributions were fit to the empirical data using maximum likelihood techniques. These distributions were selected because they can be formulated in closed-form, they are skewed distributions and it is easy to find conjugate priors for them. Fig. 4.9. shows the inverse gamma, the gamma and the log normal distribution fit to the samples along with the reference Gaussian distribution.

### 4.3.2 Measuring the distribution of receive timestamps in ultra wide band systems

---

**Thesis 3.2** – I have proposed a method to measure the distribution of the error of receive timestamps up to a constant in real ultra wide band systems, eliminating the effect of frequency drift between transceivers. I have shown that the distributions of the received timestamps are diverse and in some cases, they are not only skewed but multimodal. [C3]

---

To measure the real distribution of the receive timestamps in UWB systems, we have to synchronize the devices involved in the measurement. Assuming  $f(t) = 1$  relative frequency rate yields

$$y_k = (t_k - t_1) + \tau_{\text{ToF}} + o + \omega_k \quad (4.8)$$

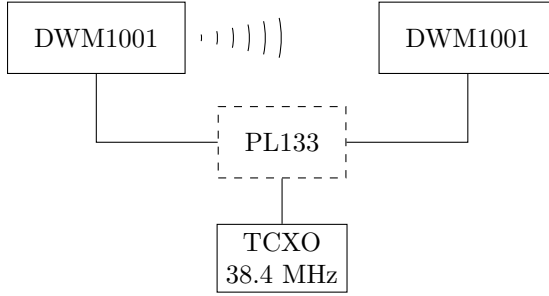


Figure 4.10: The measurement layout for the synchronized measurements. The reference clock of the thermal controlled oscillator is distributed by an extreme low additive phase noise PL133 clock distributor IC.

The quantity

$$y_k - t_k = \omega_k + (-t_1 + \tau_{\text{ToF}} + o) = \omega_k + \text{const.} \quad (4.9)$$

consists of the random variable  $\omega_k$  and a constant, if  $\tau_{\text{ToF}}$  is held constant, e.g. placing the devices to fix locations, or keeping their distance constant.

Figure 4.10 shows the layout of the measurement. The synchronization is implemented between two Decawave DWM1001 module, which are capable of sending and receiving ultra wide band signals, and precisely timestamping the transmission and reception of messages on a clock running at cca. 64GHz. To ensure  $f(t) = 1$ , the two modules are driven from a common TCXO oscillator.

Three different indoor scenarios were investigated in a university building:

1. *Calm environment*: in the evening, when little or no movement can be experienced
2. *Normal environment*: a normal workday, medium activity in the building
3. *Harsh environment*: lots of movements, high activity

The distribution of the  $\omega_k$  receive timestamps can be seen in Figure 4.11 for all the three scenarios. Note, that all the distributions are somewhat multimodal, however, the distribution in the harsh indoor environment has two very distinctive mode. It can be readily seen in the figures, that the deviation of the measurement noise increases with the activity in the building.

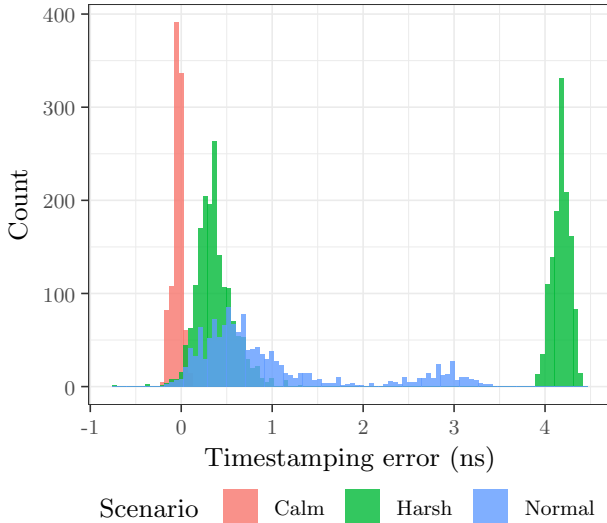


Figure 4.11: Distribution of the  $\omega_k$  measurement noise in three different measurement scenarios. The timestamping error is specified up to a constant, as in (4.9). Note, that the distribution in a harsh environment is strongly multimodal.

## 4.4 Estimating measurement noise of the distribution of the received timestamps

---

**Thesis 3.3** – I proposed a batch method to estimate the variance of the received timestamp error noise from real-life measurements to infer the frequency drift between transceivers. The method applies a third-order state model Kalman-filter along with a Bayesian smoother to estimate the optimal states, from which an Expectation-Maximalization technique estimates the measurement noise. The method increases both the accuracy and the precision of the frequency estimation compared to the classical Kalman filter-based solutions in different measurement scenarios. [C3]

---

The radio channel is generally not time-invariant – the channel impulse response can change rapidly, resulting in rapid variations in the quality of receive time estimation. This implicitly means, that the distribution of the receive timestamps changes with time, leading to varying deviation and variance. The estimation of measurement noise can substantially improve the accuracy of the state estimation.

For the dynamic model, the method uses the clock state space model (parameter-

ized by  $\sigma_1, \sigma_2, \sigma_3$ ), with  $A_k$  state transition matrix and  $\Sigma_k$  state transition covariance matrix (i.e. process dynamic noise covariance):

$$A_k = \begin{bmatrix} 1 & \Delta_k & \frac{1}{2}\Delta_k^2 \\ 0 & 1 & \Delta_k \\ 0 & 0 & 1 \end{bmatrix} \quad (4.10)$$

$$\Sigma_k = \begin{bmatrix} \sigma_1^2 \Delta_k + \sigma_2^2 \frac{\Delta_k^3}{3} + \sigma_3^2 \frac{\Delta_k^5}{20} & \sigma_2^2 \frac{\Delta_k^2}{2} + \sigma_3^2 \frac{\Delta_k^4}{8} & \sigma_3^2 \frac{\Delta_k^3}{6} \\ \sigma_2^2 \frac{\Delta_k^2}{2} + \sigma_3^2 \frac{\Delta_k^4}{8} & \sigma_2^2 \Delta_k + \sigma_3^2 \frac{\Delta_k^3}{3} & \sigma_3^2 \frac{\Delta_k^2}{2} \\ \sigma_3^2 \frac{\Delta_k^3}{6} & \sigma_3^2 \frac{\Delta_k^2}{2} & \sigma_3^2 \Delta_k \end{bmatrix} \quad (4.11)$$

where  $\Delta_k = t_k - t_{k-1}$ . The measurement model is simply

$$p(\mathbf{y}_k | \mathbf{x}_k) = \mathcal{N}(\mathbf{y}_k | H\mathbf{x}_k, \xi) \quad (4.12)$$

where

$$H = [1 \quad 0 \quad 0] \quad (4.13)$$

Assuming a known  $\xi$  measurement noise variance, the estimation of the  $\mathbf{x}_k$  states at time instant  $t_k$  in a first order Markov process can be done by using the well-known recursive Kalman-filter equations.

For latent space problems, *Expectation-Maximization* (EM) method can help to estimate the distribution of the parameter by estimating the distribution of the parameter and the latent space separately. Expectation maximization in the context of parameter estimation in latent spaces results in computing the expectation

$$Q(\xi, \xi^{(n)}) = \mathbb{E}_{\mathbf{x}_{0:K} | \mathbf{y}_{1:K}, \xi^{(n)}} [\log p(\mathbf{x}_{0:K}, \mathbf{y}_{1:K} | \xi)] \quad (4.14)$$

and then maximize it for the next iteration:

$$\xi^{(n+1)} = \arg \max_{\xi} Q(\xi, \xi^{(n)}) \quad (4.15)$$

The maximization can be achieved in a closed form. The log-likelihood of the measurement factorization – assuming an irregular, noninformative prior – is

$$\ln \mathcal{L}(\xi; \mathbf{x}_{0:K}, \mathbf{y}_{1:K}) = -\frac{K}{2} \ln |\xi| - \frac{1}{2} \sum_{k=1}^K (\mathbf{y}_k - H\mathbf{x}_k)^T \xi^{-1} (\mathbf{y}_k - H\mathbf{x}_k) + \text{const.} \quad (4.16)$$

where

$$\xi_{ML} = \frac{1}{K} \sum_{k=1}^K (\mathbf{y}_k - H\mathbf{x}_k)(\mathbf{y}_k - H\mathbf{x}_k)^T \quad (4.17)$$

For calculating  $p(\mathbf{x}_k | \mathbf{y}_{1:K})$ , the Rauch-Tung-Striebel smoother can be applied.

---

**Algorithm 1** Step for the joint estimation of the clock state  $\mathbf{x}_k$  and the measurement noise variance  $\xi_k$  at timestep  $k$ .  $\text{KF}(\cdot)$  represents Kalman-filtering, while  $\text{RTS}(\cdot)$  represents Rauch-Tung-Striebel smoothing.

---

**Input:**

- $k$ : Actual timestep index
- $N_{EM}$ : Expectation-Maximization iteration count
- $W$ : Window size
- $A_{(k-W):k}$ : Last  $W$  dynamic matrices
- $H_{(k-W):k}$ : Last  $W$  measurement matrices
- $\mathbf{x}_{(k-W):(k-1)}$ : Last  $W - 1$  state means
- $P_{(k-W):(k-1)}$ : Last  $W - 1$  covariance matrices
- $\sigma_1^2, \sigma_2^2, \sigma_3^2, \xi_k$ : Actual dynamic and measurement noise variances
- $\mathbf{y}_{(k-W):k}$ : Last  $W$  measurements

**Output:**

- $\mathbf{x}_k, P_k$ : Actual state
- $\omega_k^2$ : Estimated measurement noise variance

**Procedure**

- 1:  $\mathbf{x}_k, P_k \leftarrow \text{KF}(\mathbf{x}_{k-1}, P_{k-1}, A_k, H_k, \sigma_1^2, \sigma_2^2, \sigma_3^2, \xi_k)$
  - 2: **for**  $i \leftarrow 1$  **to**  $N_{EM}$  **do**
  - 3:  $\mathbf{x}_{(k-W):k}^{RTS} \leftarrow \text{RTS}(W, \mathbf{x}_{(k-W):k}, P_{(k-W):k})$
  - 4:  $\omega_k^2 \leftarrow \frac{1}{W} \sum_{i=k-W}^k (\mathbf{y}_i - H_i \mathbf{x}_i^{RTS})^2$
  - 5:  $\mathbf{x}_{(k-W):k}, P_{(k-W):k} \leftarrow \text{KF}(\mathbf{x}_{k-W}, P_{k-W}, A_{(k-W):k}, H_{(k-W):k}, \sigma_1^2, \sigma_2^2, \sigma_3^2, \xi_k)$
  - 6: **end for**
  - 7: **return**  $\mathbf{x}_k, P_k, \xi_k$
-

The summary of the algorithm can be found in Algorithm 1 for a  $W$  wide window of measurements. The algorithm estimates the measurement noise variance and the clock state at timestep  $k$  based on the last  $W$  measurements.

Figure 4.12 shows the absolute frequency drift errors as empirical commulative distribution functions. The Kalman-filter with the estimated measurement noise act better than the original Kalman-filter solution in all scenarios. Note, that in the case of the calm and normal scenario, the difference between the optimal Kalman-filter and the original one is very small, however, using the optimal measurement noise results in fewer overshoots (i.e. smaller deviation).

## 4.5 Precise time synchronization in IEEE 802.1AS systems

---

**Thesis Group 4** – I have derived the time-invariant measurement model of Precision Time Protocol in order to apply adaptive Kalman filtering for synchronizing remote clocks. I have shown, that adaptive Kalman filtering outperforms existing Kalman filtering-based algorithms for Precision Time Protocol both in accuracy and precision. [J2]

---

The thesis group’s primary contribution is introducing a measurement model featuring time-invariant noise covariance. Building upon this model, the chapter proposes a computationally feasible Adaptive Kalman Filtering algorithm grounded in optimal Bayesian estimation. This algorithm aims at online prediction of packet delay variation in the IEEE 1588 protocol. The adaptive approach leads to both enhanced precision, thereby reducing estimation variance, and improved accuracy by mitigating bias.

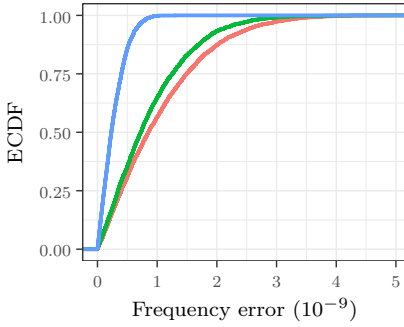
### 4.5.1 Measure packet delay variation in IEEE 1588 network

---

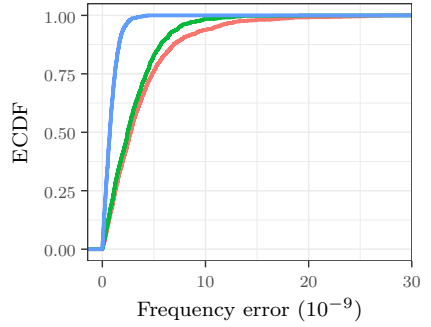
**Thesis 4.1** – I have proposed a method to measure the distribution of the error of received timestamps using the Precision Time Protocol (PTP). My analysis shows that the range of these distributions depends on both the network configuration and its operation. The analysis reveals that even under typical operating scenarios, the variance of the distributions can vary significantly in magnitude, making accurate a priori estimation particularly challenging. [J2]

---

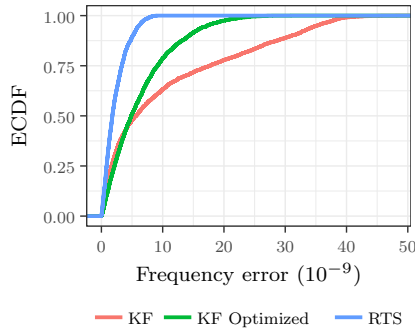
Since the relative running of the clocks of two or more devices is unknown, it is hard to acquire the ground-truth values for the results to be comparable. To



(a) Calm environment



(b) Normal environment



(c) Harsh indoor environment

Figure 4.12: The empirical cumulative distribution of the absolute error between the estimated relative frequency and the ground truth relative frequency of the slave device in different measurement scenarios. In all scenarios, the green curve of the noise optimized Kalman-filter gives better results, especially in the case of strong multipath propagation. For reference, the optimal Bayes-estimation, the result of the RTS smoother is presented in blue.

overcome this issue, two ports of an ESPRESSObin v7 device were used to be the PTP master and the PTP slave, since ESPRESSObin has one and the same clock for all PTP ports. To trick the Linux operating system to send the packets onto the wire instead of a local shortcut, for which simple firewall and ARP rules were applied. This way, the ground-truth time at the reception of a *Sync* message is the same as the RX timestamp, providing ground-truth values for the clock estimation. The hardware clock of the ESPRESSObin runs on 125MHz providing 8ns clock resolution.

The measurements were carried out in 6 different scenarios. Two switches were applied, and 6 scenarios differ in the network setup and in the amount of background traffic. The scenarios are as follows:

1. Using the Cisco switch to connect the master and the slave, no background traffic.
2. Using the Cisco switch to connect the master and the slave, with 100 Mbps independent bidirectional background traffic.
3. Using two switches with independent 100 Mbps bidirectional background traffic.
4. Using two switches with independent 50 Mbps bidirectional background traffic.
5. Using two switches without background traffic.
6. Using the department network between ESPRESSObin's ports on a typical workday.

Figure 4.13 shows the distributions of the packet delays separately for the *Sync* and the *Delay response* messages. It is clearly visible that the scenarios provide rather different packet delay distributions, both in variance and shape. E.g. Scenario 4 shows strong asymmetric distribution as can be seen on its violin plot, while in Scenarios 1-3, *Sync* messages have nearly uniform delay distributions with different variances. Also, it is clear that the packet delays are strongly asymmetric in the sense of the IEEE 1588, i.e. *Sync* and *Delay response* messages has different expected delays. However, the focus is on the variance mainly, so to handle the issue of the asymmetry, the numerous methods proposed in the literature can be applied.

## 4.5.2 Time-invariant measurement model for adaptive filtering

---

**Thesis 4.2** – I have proposed a probabilistic measurement model for Precision Time Protocol with time-invariant measurement noise variance to provide compatibility with the Adaptive Kalman Filter (AKF). I have shown, that in the proposed model both state variables are observable.[J2]

---

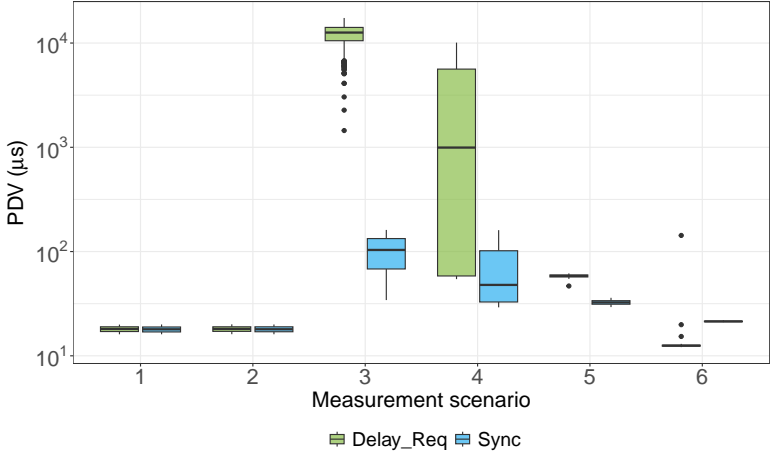


Figure 4.13: Packet delay distributions (PDV) in different scenarios as box plots (note the logarithmic axis). In most cases, the forward-backward distributions are strongly asymmetric with extensive difference in noise variance.

Assuming a PTP message exchange, let  $t_k^1$  the TX timestamp for the  $k$ th *Sync* message, and  $t_k^4$  is the RX timestamp for the *Delay\_Req* message. Let  $\tau_k^2$  and  $\tau_k^3$  the RX timestamp of the *Sync* and the TX timestamp of the *Delay\_Req* message, respectively, measured by the local clock of the slave device. The measurement equation in a two state model can be written as

$$\frac{t_k^{(1)} + t_k^{(4)}}{2} = H_k \mathbf{x}_k + r_k \quad (4.18)$$

with

$$H_k = \left[ 1 \quad \frac{1}{2}(\tau_k^{(3)} - \tau_k^{(2)}) \right] \quad r_k = \frac{\varepsilon}{2} + \frac{\xi_{PDV}^{(4)} + \xi_{PDV}^{(2)}}{2}$$

and  $\varepsilon \sim \mathcal{N}(0; \sigma_\varepsilon^2)$  with  $\sigma_\varepsilon^2 = \sigma_\theta^2(\tau_k^{(3)} - \tau_k^{(2)}) + \sigma_\gamma^2 \frac{(\tau_k^{(3)} - \tau_k^{(2)})^3}{3}$ . The  $\varepsilon$  noise is the effect of the uncertainty of the drift of the local clock while estimating the real delay between  $t^2$  and  $t^3$ , while noises  $\xi_{PDV}^{(4)}$ ,  $\xi_{PDV}^{(2)}$  are the result of the packet delay variation. The measurement noise depends on the time step only through the response time, and the three noise sources are considered to be independent, so the variance can be calculated as

$$\begin{aligned} R &= \text{Var} [r_k^2] = \text{Var} \left[ \frac{\varepsilon}{2} \right] + \text{Var} \left[ \frac{\xi_{PDV}^{(4)} + \xi_{PDV}^{(2)}}{2} \right] = \\ &= \sigma_\theta^2 \frac{\tau_k^{(3)} - \tau_k^{(2)}}{4} + \sigma_\gamma^2 \frac{(\tau_k^{(3)} - \tau_k^{(2)})^3}{12} + \frac{\sigma_\xi^2}{2} \approx \frac{\sigma_\xi^2}{2} \end{aligned} \quad (4.19)$$

Since the response time in real systems is in the order of milliseconds, the contribution of the clock noise  $\varepsilon$  can be ignored, resulting in a measurement noise effectively being time invariant. For the approximation, we assume that  $\text{Var}[\xi_{PDV}^4] = \text{Var}[\xi_{PDV}^2] = \sigma_\xi^2$ , and the noises are independent. Both the states are observable since the matrix

$$O = \begin{bmatrix} H_k \\ A_k H_k \end{bmatrix} = \begin{bmatrix} 1 & \frac{1}{2} \Delta_k \\ 1 & \frac{3}{2} \Delta_k \end{bmatrix}$$

has full-rank for every  $\Delta_k \neq 0$ .

### 4.5.3 Evaluation of the proposed algorithm

---

**Thesis 4.3** – I have proposed an online time synchronization algorithm based on Adaptive Kalman Filtering using the measurement model of Thesis 4.2. I have compared the Adaptive Kalman Filtering-based algorithm with different state-of-the-art clock state estimation algorithms, and I have shown that the AKF has a performance close to the optimal filtering with a computational complexity close to classic Kalman filtering. [J2]

---

Using the covariance estimate of the Kalman-filter innovations for a  $W$  wide window, i.e.

$$\hat{S} = \frac{1}{W} \sum_{i=1}^W \hat{\mathbf{v}}_i \hat{\mathbf{v}}_i^T \quad (4.20)$$

in the Adaptive Kalman Filter (AKF), the measurement noise covariance matrix can be estimated as

$$\hat{R} = \hat{S} - H_k P_k^- H_k^T$$

with  $H_k$  being the observation matrix at the  $k$ th time step, and  $P_k^-$  is the estimated a priori state covariance matrix.

The AKF was evaluated using simulations (with gaussian and exponential noises) and real-data recorded by the method presented in Thesis 4.1. The results were compared to the following clock state estimation algorithms:

**TH** The theoretically optimal Kalman filter.

**KF** The Kalman-filter defined in [12].

**KF-HN** Also [12] with  $\sigma_{\theta_M} = 10^{-4}$ s

**M-robust** Robust and adaptive Kalman filter defined in [13].

**KF-EM** Expectation-maximization based optimal Kalman filter defined in Thesis 2.3.

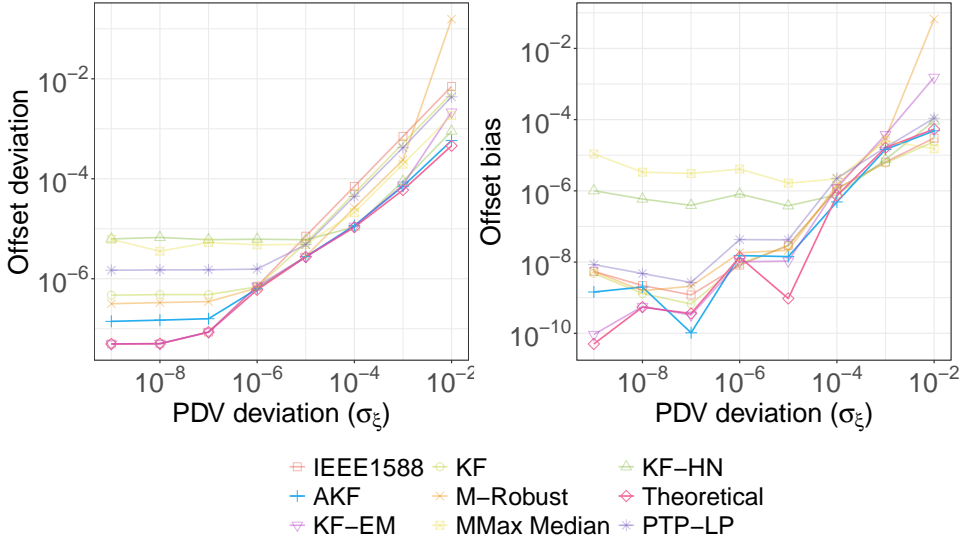


Figure 4.14: The deviation (left) and bias (right) of the master-slave offset estimation at different measurement noise deviations using normal distribution ( $\sigma_\theta = 10^{-6}$ s,  $\sigma_\gamma = 10^{-8}$ ).

**MMax** Minimax technique [14] with median statistics

**PTP-LP** PTP-LP linear programming based method using the PTP-H heuristics [15].

The results can be seen in Figure 4.14, 4.15, 4.16. The AKF based estimation is very close to the theoretical performance, and only comparable to the EM based solution, which is computationally much more complex algorithm.

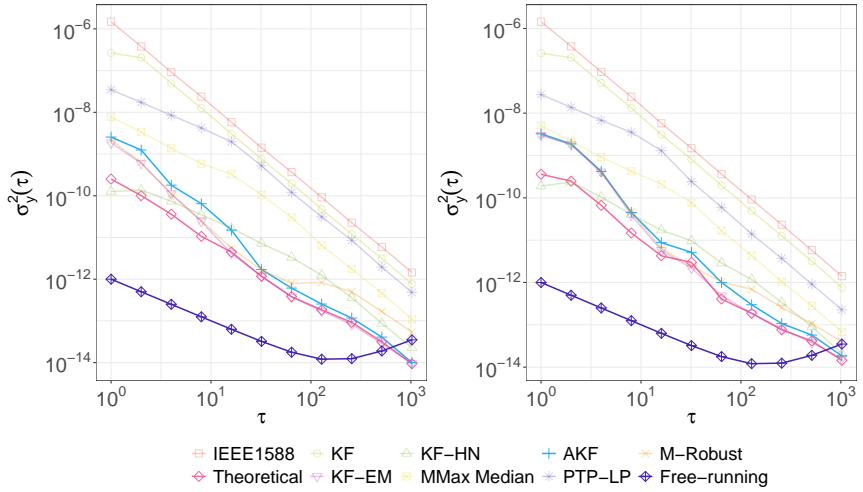


Figure 4.15: The overlapped Allan variance plots of the estimators in simulation for normally (left) and exponential (right) distributed measurement noise with  $\sigma_\xi = 10^{-3}$ s. For reference, the plots depict the theoretical Allan deviation of the free-running clock. ( $\sigma_\theta = 10^{-6}$ s,  $\sigma_\gamma = 10^{-8}$ )

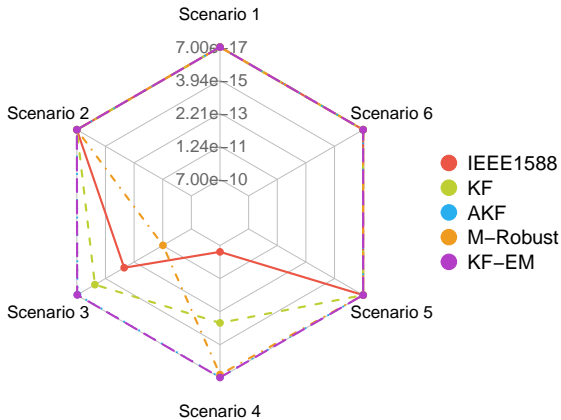


Figure 4.16: Overlapped Allan variance of different estimators at different measurement scenarios at  $\tau = 128$ s.

# Applicability of the results

Most of the outcomes from the research efforts constitute applied research, which emphasizes practical applications and ensures that the findings are easily adaptable for real-world use. This focus on applied research allows the algorithms to be implemented more efficiently, serving specific needs in both industry and technology development. For instance, the findings from Thesis groups 1 and 3 were directly applied to a project titled „Development of mass sport supporting sensor device and analytical service” (2018-1.1.1-MKI-2018-00075). The aim of this project was to enhance the performance of tracking systems by improving measurement frequency and optimizing the overall tracking capabilities. These innovations play a significant role in advancing technologies that support large-scale sports activities, ultimately providing more precise data collection and analysis.

On the other hand, the results from Thesis groups 2 and 4 hold wider implications, particularly in the domain of clock state estimation, which is crucial in clock servo implementations. These findings have the potential to significantly contribute to projects such as the PTPd project [16] and The Linux PTP Project [17], both of which are fundamental in the precise synchronization of clocks in distributed systems. The importance of accurate clock synchronization cannot be overstated in fields such as telecommunications, networked control systems, and various time-sensitive applications where performance depends on reliable timekeeping.

Furthermore, the work from Thesis group 4 stands out due to its low computational complexity, which is particularly advantageous when considering resource-constrained environments. This characteristic makes it feasible to implement their discoveries in embedded systems that have limited processing power and memory. As a result, these solutions can be deployed in a variety of small, portable devices without compromising on efficiency or performance, expanding their applicability to numerous embedded systems across various industries, including automotive, industrial automation, and consumer electronics.

# Bibliography

- [1] Oscar Seijo, Jesus Alberto Lopez-Fernández, Hans-Peter Bernhard, and Inaki Val. Enhanced Timestamping Method for Subnanosecond Time Synchronization in IEEE 802.11 Over WLAN Standard Conditions. *IEEE Transactions on Industrial Informatics*, 16(9):5792–5805, 2020.
- [2] Zeba Idrees, Jose Granados, Yang Sun, Shahid Latif, Li Gong, Zhuo Zou, and Lirong Zheng. IEEE 1588 for Clock Synchronization in Industrial IoT and Related Applications: A Review on Contributing Technologies, Protocols and Enhancement Methodologies. *IEEE Access*, 8:155660–155678, 2020.
- [3] IEEE Standard for a Precision Clock Synchronization Protocol for Networked Measurement and Control Systems. *IEEE Std 1588-2019 (Revision of IEEE Std 1588-2008)*, pages 1–499, 2020.
- [4] Jose A. del Peral-Rosado, Olivier Renaudin, Christian Gentner, Ronald Raulefs, Enrique Dominguez-Tijero, Alejandro Fernandez-Cabezas, Fernando Blazquez-Luengo, Gema Cueto-Felgueroso, Alexander Chassaigne, David Bartlett, Florin Grec, Lionel Ries, Roberto Prieto-Cerdeira, Jose A. Lopez-Salcedo, and Gonzalo Seco-Granados. Physical-Layer Abstraction for Hybrid GNSS and 5G Positioning Evaluations. In *2019 IEEE 90th Vehicular Technology Conference (VTC2019-Fall)*, pages 1–6, 2019.
- [5] Marco Martalò, Simone Perri, Gianmichele Verdano, Francesco De Mola, Francesco Monica, and Gianluigi Ferrari. Improved UWB TDoA-Based Positioning Using a Single Hotspot for Industrial IoT Applications. *IEEE Transactions on Industrial Informatics*, 18(6):3915–3925, 2022.
- [6] Johannes Friedrich, Janis Tiemann, and Christian Wietfeld. Accurate Multi-Zone UWB TDOA Localization utilizing Cascaded Wireless Clock Synchronization. In *2021 International Conference on Indoor Positioning and Indoor Navigation (IPIN)*, pages 1–8, 2021.
- [7] Yun Cheng and Taoyun Zhou. UWB Indoor Positioning Algorithm Based on TDOA Technology. In *2019 10th International Conference on Information Technology in Medicine and Education (ITME)*, pages 777–782, 2019.
- [8] Federico Bonafini, Paolo Ferrari, Alessandra Flammioni, Stefano Rinaldi, and Emiliano Sisinni. Exploiting Time Synchronization as Side Effect in UWB Real-Time Localization Devices. In *2018 IEEE International Symposium on Precision Clock Synchronization for Measurement, Control, and Communication (ISPCS)*, pages 1–6, 2018.

- [9] Mohsin Raza, Nauman Aslam, Hoa Le-Minh, Sajjad Hussain, Yue Cao, and Noor Muhammad Khan. A Critical Analysis of Research Potential, Challenges, and Future Directives in Industrial Wireless Sensor Networks. *IEEE Communications Surveys Tutorials*, 20(1):39–95, 2018.
- [10] Ken Peppers, Tuure Tuunanen, Marcus Rothenberger, and S. Chatterjee. A design science research methodology for information systems research. *Journal of Management Information Systems*, 24:45–77, 01 2007.
- [11] Andreas F. Molisch, Kannan Balakrishnan, Dajana Cassioli, Chia-Chin Chong, Shahriar Emami, Andrew Fort, Johan, Karedal, Juergen Kunisch, Hans Gregory Schantz, Ulrich G. Schuster, and Kai Siwiak. IEEE 802.15.4a channel model-final report. 2004.
- [12] Giada Giorgi and Claudio Narduzzi. Performance Analysis of Kalman-Filter-Based Clock Synchronization in IEEE 1588 Networks. *IEEE Transactions on Instrumentation and Measurement*, 60(8):2902–2909, 2011.
- [13] Z.M. Durovic and B.D. Kovacevic. Robust estimation with unknown noise statistics. *IEEE Transactions on Automatic Control*, 44(6):1292–1296, 1999.
- [14] Anand Guruswamy, Rick S. Blum, Shaline Kishore, and Mark Bordogna. Minimax Optimum Estimators for Phase Synchronization in IEEE 1588. *IEEE Transactions on Communications*, 63(9):3350–3362, 2015.
- [15] Henning Puttnies, Peter Danielis, and Dirk Timmermann. PTP-LP: Using Linear Programming to Increase the Delay Robustness of IEEE 1588 PTP. In *2018 IEEE Global Communications Conference (GLOBECOM)*, pages 1–7, 2018.
- [16] GitHub - ptpd/ptpd: PTPd official source - master branch a.k.a. trunk — github.com. <https://github.com/ptpd/ptpd>. [Accessed 05-09-2024].
- [17] The Linux PTP Project — linuxptp.sourceforge.net. <https://linuxptp.sourceforge.net/>. [Accessed 05-09-2024].

# Publications

## Journal papers

- [J1] Gergely Hollósi and István Moldován. Ultra Wideband-based wireless synchronization of IEEE 1588 clocks. *Infocommunications Journal*, 15(2):21–28, 2023.
- [J2] Gergely Hollósi and Dániel Ficzer. Adaptive Kalman Filtering in Offset Estimation for Precision Time Protocol. *IEEE Transactions on Industrial Informatics*, 21(1):396–404, 2025.
- [J3] Gergely Hollósi, Csaba Lukovszki, István Moldován, Sándor Plósz, and Frigyes Harasztos. Monocular indoor localization techniques for smartphones. *Acta Universitatis Sapientiae, Informatica*, 8(2):186–215, 2016.
- [J4] Gergely Hollósi, Csaba Lukovszki, Máté Bancsics, and Gábor Magyar. Traffic Swarm Behaviour: Machine Learning and Game Theory in Behaviour Analysis. *Infocommunications Journal*, 13(4):19–27, 2021.
- [J5] Gergely Hollósi, Csaba Lukovszki, István Moldován, Sándor Plósz, and Frigyes Harasztos. Survey on Monocular Odometry for Conventional Smartphones. *Infocommunications Journal*, page 25, 2016.
- [J6] Attila Frankó, Gergely Hollósi, Dániel Ficzer, and Pal Varga. Applied Machine Learning for IIoT and Smart Production and Methods to Improve Production Quality, Safety and Sustainability. *Sensors*, 22(23), 2022.

## Conference proceedings

- [C1] Gergely Hollósi, Csaba Lukovszki, and Máté Bancsics. Radio Resource Efficient UWB Measurement System Design and Performance Analysis for TWR-based Ranging. In *2022 IEEE 5th International Conference on Industrial Cyber-Physical Systems (ICPS)*, pages 1–6, 2022.
- [C2] Gergely Hollósi. Distribution of ultra wideband (UWB) receive timestamps in dense indoor environment based on the Saleh-Valenzuela channel model. In *2022 14th International Conference on Communications (COMM)*, pages 1–5, 2022.

- [C3] Gergely Hollósi. Bayesian Measurement Noise Estimation in Ultra Wide Band Systems for Clock Synchronization. In *2023 IEEE 19th International Conference on Factory Communication Systems (WFCS)*, pages 1–8, 2023.
- [C4] Sándor Plósz, Zsolt Kertész, Csaba Lukovszki, Dávid Kovács, István Moldován, and Gergely Hollósi. Practical aspects of visual recognition for indoor mobile positioning. In *2013 IEEE 4th International Conference on Cognitive Infocommunications (CogInfoCom)*, pages 527–532, 2013.
- [C5] Sándor Plósz, Csaba Lukovszki, and Gergely Hollósi. Visual feature recognition based indoor localization. In *1st International Conference and Exhibition on Future RFID Technologies*, pages 143–150. Eszterházy Károly Főiskola, 11 2014.
- [C6] Dániel Ficzer, Gergely Hollósi, Attila Frankó, and András Gulyás. Random walk for generalization in goal-directed human navigation on Wikipedia. In *The 11th International Conference on Complex Networks and their Applications*, 06 2022.
- [C7] Attila Frankó and Gergely Hollósi. Settling Issues in IEEE 802.1AS Networks in PI Based Clock Servos. In *2023 19th International Conference on Network and Service Management (CNSM)*, pages 1–7, 2023.
- [C8] Dániel Ficzer, Gergely Hollósi, Attila Frankó, and András Gulyás. Random Walk for Generalization in Goal-Directed Human Navigation on Wikipedia. In Hocine Cherifi, Rosario Nunzio Mantegna, Luis M. Rocha, Chantal Cherifi, and Salvatore Miccichè, editors, *Complex Networks and Their Applications XI*, pages 202–213, Cham, 2023. Springer International Publishing.
- [C9] Dániel Ficzer, Gergely Hollósi, and Pál Varga. Live traffic analysis on S1-MME interface using LSTM autoencoder. In *2023 IEEE International Mediterranean Conference on Communications and Networking (MeditCom)*, pages 68–73, 2023.
- [C10] Dániel Ficzer, Gergely Hollósi, Attila Frankó, and Pál Varga. AI Toolbox Concept for the Arrowhead Framework. In *2023 19th International Conference on Network and Service Management (CNSM)*, pages 1–7, 2023.
- [C11] Dániel Ficzer, Gergely Hollósi, Attila Frankó, Pál Varga, and József Biró. Orderliness of Navigation Patterns in Hyperbolic Complex Networks. In Hocine Cherifi, Luis M. Rocha, Chantal Cherifi, and Murat Donduran, editors, *Complex Networks & Their Applications XII*, pages 271–282, Cham, 2024. Springer Nature Switzerland.
- [C12] D. Ficzer, G. Hollósi, A. Frankó, P. Varga, and J. Biró. The Traveling Salesman Problem on the Hyperbolic Plane. In *2023 International Conference*

on *Computational Science and Computational Intelligence (CSCI)*, pages 433–437, 2023.

- [C13] Gergely Hollósi, Dániel Ficzer, Attila Frankó, Máté Bancsics, Ruba AlMahasneh, Csaba Lukovszki, and Pál Varga. AIMS5.0 AI Toolbox: Enabling Efficient Knowledge Sharing for Industrial AI. In *NOMS 2024-2024 IEEE Network Operations and Management Symposium*, pages 1–6, 2024.
- [C14] Gergely Hollósi, Dániel Ficzer, and Pál Varga. Generative AI for Low-Level NETCONF Configuration in Network Management Based on YANG Models. In *2024 20th International Conference on Network and Service Management (CNSM)*, pages 1–7, 2024.
- [C15] Ruba AlMahasneh, Gergely Hollósi, Dániel Ficzer, Máté Bancsics, Csaba Lukovszki, and Pál Varga. Uncovering Common AI Challenges Across Industrial Domains in the Transition to Industry 5.0. In *2024 20th International Conference on Network and Service Management (CNSM)*, pages 1–7, 2024.